Received: 22 July 2021 | Revised: 21 July 2022 | Accepted: 11 August 2022

IET Power Electronics

DOI: 10.1049/pel2.12381

The Institution of Engineering and Technology WILEY

ORIGINAL RESEARCH

Modelling and indirect field-oriented control for pole phase modulation induction motor drives

Atif Iqbal[1] | **B. Prathap Reddy**[2] | **Syed Rahman**[3] | **Mohammad Meraj**[4]

[1]Department of Electrical Engineering, Qatar University, Doha, Qatar

[2]Department of Electronic Systems Engineering, Indian Institute of Science, Bengaluru, Karnataka, India

[3]Department of Electrical Engineering, Texas A&M University, College Station, Texas, USA

[4]Department of Electronics and Electrical Engineering, University of Strathclyde, Glasgow, Scotland

Correspondence
Atif Iqbal, Department of Electrical Engineering, Qatar University, BCR-F203 P.O. Box-2713, Doha, Qatar.
Email: atif.iqbal@qu.edu.qa

Abstract

In the recent days, for the traction and electric vehicle (EV) applications, multiphase machines with pole phase modulation (PPM) technique have been proposed. The smoother operation during pole changeovers as well as steady-state operations is a significant constraint while adopting the PPM-based multiphase induction motor (PPMIM) drives for EV and traction applications. So, in this paper, the PPMIM dynamic model and associated vector control are proposed for attaining a smoother operation of the machine. The machine modelling equations and transformation matrices are implemented in an arbitrary reference frame by considering the different pole phase combinations. Based on the modelling equations, the indirect field-oriented control (IFOC) is proposed for PPMIM drives by reflecting the associated changes in parameters for different pole phase modes. In the IFOC, for regulating the *d*-axis and *q*-axis current components, single PI control loops have been implemented for all pole-phase combinations. The proposed IFOC scheme is robust and applicable for adopting any type of pulse width modulation. The experimental, as well as simulation results, are given to illustrate the potentiality of the proposed dynamic model and IFOC. The PPMIM machine performance during the steady state as well as pole changeovers in different pole phase modes are analyzed and associated. Simulation and experimental results are presented.

1 | INTRODUCTION

HE multiphase inverter-driven multiphase induction motors have seen a predominant growth in the present century due to higher efficiency, highly reliable operation, lower-rated resources, lesser torque ripple, and better power/torque sharing [1–6]. In addition to this, the technological advancements in power electronics and the necessity of efficient systems have further boosted the interest on multiphase machines in high power applications as a substitute for traditional three-phase systems [2]. Typical examples include wind energy systems with arbitrary power-sharing [3], electric traction with gearless operation [4], AC on-board fast charging for electric vehicles (EVs) [5], and ship propulsion systems with improved fault tolerance [6] and electric aircraft [2].

In [7–13], pole phase modulated induction motor (PPMIM) drives for electric traction are reported with the advent of multiphase machines, where the flexibility of an additional degree of freedom is effectively used. A 3:1 pole changeable 9-phase machine, 1:3:5 pole changeable 15-phase machine, 1:3:5:9:10 pole changeable 45-phase machine and other multiphase machines are presented based on pole phase modulation (PPM) techniques [7–13]. The multiphase PPMIM drives offer a speed-torque profile similar to the conventional 'IC engine + gearbox' system, which results in the removal of the gearbox system for EVs and traction applications [4, 9]. The speeds, as well as torques of a machine, are changed appropriately by regulating the number of poles as well as phases without changing the stator winding terminals [7]. The torque generated by the induction machine is directly proportional to the number of poles of the machine ($T \propto P$) [2]. Based on this relation, in high pole mode, the PPMIM drive delivers higher torque as compared to low pole mode, but the increment in the number of poles results in a reduction in magnetizing inductance, higher magnetizing current, higher torque ripple, lower power factor as well as efficiency [14, 15]. The performance improvement of the PPMIM drive with different multilevel inverter structures, phase grouping concepts and carrier phase shifted

PWMs are presented in [10–13]. In these works, the control of PPMIM machines during pole changeovers has not been discussed. Therefore, there is a necessity to implement a simple control technique for controlling the PPMIM drive with smooth transitions during different pole-phase changeovers.

The modelling and control techniques of multiphase machines are similar to the 3-phase machines reported in [2], [16–23]. For sinusoidally distributed machines with any number of phases the modelling equations, as well as vector control techniques, are the same, that is, the first fundamental *dq* components are responsible for the torque production and drive control [2], [16, 17]. However, the transformation matrix for an m phase machine is $m \times m$, where the matrix consists of $(m-1)/2$ and $(m-2)/2$ sub-planes for odd and even numbers of phase machines, respectively. The mathematical modelling and different vector control techniques for 5-phase machines [17, 18], 6-phase machines [19–21], 7-phase machines [22], 9-phase machines [23], and other multiphase machines are presented in [2], [16–23] for accurate and fast control of torque/speed. In this literature, the authors have focused on indirect field-oriented control (IFOC) because of its simplicity in control, ease of extension for a machine with any number of phases, decoupled control of torque and speed, robust nature, etc. [2, 16]. Based on this literature, an IFOC is implemented for a 9-phase PPMIM machine with a 1:3 ratio of torque/speed change in [8], [24–26], where the basic modelling and control are presented according to 3-phase machine analysis that is presented. However, in this literature, the authors have implemented individual control loops and modelling equations for 9phase 4pole mode (9PH-4PO) and 3phase 12pole (3PH-12PO) modes, that is, two models have been implemented. Moreover, the transformation matrices are not symmetrical (i.e. 4–9 is implemented) and the control, as well as the behaviour of the machine during the pole changeover, has not been explored. In addition to this, the control is implemented with multiple PI control loops, which results in sensitive tuning as well as huge currents in transients. In [27] modelling and hysteresis control for 9-phase machines are implemented, but, the limitations are unregulated switching frequency, current-based control, and transient behaviour.

To address the concerns of modelling and control during the pole-phase changeover, this paper presents a single mathematical model and control of a 9-phase PPMIM drive is presented. The key contributions of this paper are,

- Modelling equations in an arbitrary reference frame are presented, where both 9PH-4PO and 3PH-12PO mode equations are combined into a single mathematical model in accordance with the control variables.
- A simple voltage-based IFOC for a 9-phase PPMIM drive is implemented for controlling the torque/speed.
- Control is implemented with a single PI loop for torque as well as flux control of a machine in all pole phase combinations.
- Robust IFOC structure with less sensitivity on PI tuning due to the lesser number of PI loops over control schemes is given in [8, 24, 27].

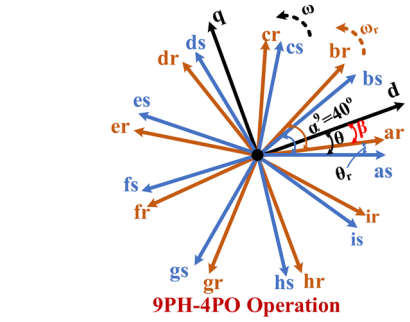

(a)

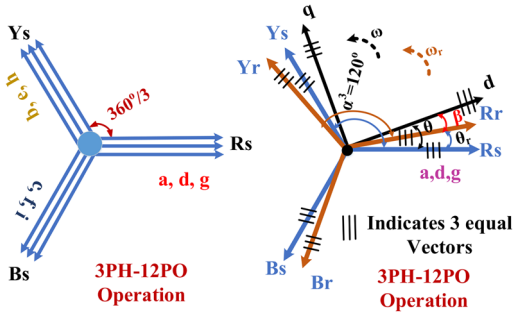

(b)

9PH-4PO Operation

Slot Number	1	2	3	4	5	6	7	8	9	10	11	12	13	14	15	16	17	18
Phase Current	a	*f	b	*g	c	*h	d	*i	e	*a	f	*b	g	*c	h	*d	i	*e
Slot Angle	0	20	40	60	80	100	120	140	160	180	200	220	240	260	280	300	320	340
Poles	N									S								

3PH-12PO Operation

Slot Number	1	2	3	4	5	6	7	8	9	10	11	12	13	14	15	16	17	18
Phase Current	R	*B	Y	*R	B	*Y	R	*B	Y	*R	B	*Y	R	*B	Y	*R	B	*Y
Slot Angle	0	60	120	180	240	300	0	60	120	180	240	300	0	60	120	180	240	300
Poles	N			S			N			S			N			S		

*Slot Angle in electrical degrees

(c)

FIGURE 1 Vector distribution of 9-phase PPMIM (*s* represents stator side and *r* represents rotor side), (a) $\alpha^9 = 40°$ for 9PH-4PO mode, (b) $\alpha^3 = 120°$ for 3PH-12PO mode, (c) machine winding details for 50% of stator circumference. PPMIM, pole phase modulation induction motor.

- Transient current magnitudes during pole changeover are minimized over [8, 24, 27].
- Fixed switching frequency of operation, which is applicable to implement any PWM.
- The transient operation of the PPMIM drive during pole changeovers is accurately controlled.

The proposed modelling equations and IFOC are validated in both simulation (MATLAB) and hardware (on a 5 hp laboratory prototype).

2 | MULTIPHASE POLE PHASE MODULATED INDUCTION MOTOR MODELLING

The schematic vector distribution of the 9-phase PPMIM drive is shown in Figure 1. The winding design of the 9-phase PPMIM machine is presented in Figure 1c, and the detailed generalization, and guidelines of PPM are given in [7–13]. In a 36-slot PPMIM drive, the stator windings are designed for 9PH-4PO

operation, that is, sinusoidally distributed with a phase shift of 40°, as shown in Figure 1. In this figure, it can be visualized that, the same phase windings are excited with 120° phase shifts to obtain the 3PH-12PO winding configuration. In the literature [10–13], phase grouping concepts are reported to PPMIM drives for enhancing the performance of the drive as well as for simple visualization of operation. According to this phase grouping, in 9PH-4PO mode, the stator windings are grouped as three-phase winding sets (each group has three 120° displaced windings). In 3PH-12PO mode the windings in each group require the same fundamental voltage, that is, *a, d*, and *g* windings are identical voltage windings. The resultant voltage vectors for stator windings are shown in Figure 1b, that is, R-phase with *a*, *d*, *g* windings, Y-phase with *b*, *e*, *h* windings, and Z-phase with *c*, *f*, *i* windings. Similar to the stator, rotor windings are also distributed sinusoidally with the respective phase shifts in different pole phase modes. In the paper, a squirrel cage rotor induction motor is considered, that is, the rotor bars are shorted, and the voltages of rotor windings are zero.

In the designing of modelling equations for PPMIM drives the following assumptions are considered: (i) All phase windings are symmetrically distributed over a stator circumference with an angle of $2\pi/9$ degrees in 9PH-4PO mode and $2\pi/3$ in 3PH-12PO mode and (ii) machine has uniform airgap, MMF, as well as flux distribution in the air gap of the machine is purely sinusoidal without any harmonics. The other assumptions (i.e. slotting effects, losses, non-linearities of core, and others) are considered the same as conventional machine modelling [1, 16–28].

The modelling of a 9-phase PPMIM drive consists of 9PH-4PO as well as 3PH-12PO mode equations, that is,

$$9-Phase\ PPMIM\ Drive = S_1 x + S_2 y \tag{1}$$

where S_1 and S_2 define the mode of operation, that is, $S_1 = 1$, $S_2 = 0$ for 9PH-4PO mode, $S_1 = 0$, $S_2 = 1$ for 3PH-12PO mode, and $S_1 = 1$, $S_2 = 1$ both modes will exist at the same time during pole changeovers (transient condition). The variables x and y are mathematical equations of the respective pole phase mode.

The voltage equations in the phase variable domain for the PPMIM drive are,

$$\begin{bmatrix} V_{ms}^{z} \\ V_{mr}^{z} \end{bmatrix} = \begin{bmatrix} R_{ms} & \\ & R_{mr} \end{bmatrix} \begin{bmatrix} i_{ms}^{z} \\ i_{mr}^{z} \end{bmatrix} + p \begin{bmatrix} [L_s]_{m*m}^{z} & [L_{sr}]_{m*m}^{z} \\ \left[[L_{sr}]_{m*m}^{z}\right]^T & [L_r]_{m*m}^{z} \end{bmatrix} \begin{bmatrix} i_{ms}^{z} \\ i_{mr}^{z} \end{bmatrix} \tag{2}$$

In Equation (2), voltage and currents are column matrices,

$$\begin{aligned} \left[f_{mn}^{z}\right] = S_1 \left[f_{an}^{9} \quad f_{bn}^{9} \quad f_{cn}^{9} \quad f_{dn}^{9} \ldots\ldots\ldots f_{in}^{9}\right]^T \\ + S_2 \left[f_{an}^{3} \quad f_{bn}^{3} \quad f_{cn}^{3} \quad f_{dn}^{3} \ldots\ldots\ldots f_{in}^{3}\right]^T \end{aligned} \tag{3}$$

where m represents phases, $m = a, b, c \ldots I$, and n represent either stator or rotor variables, $n = s, r$. The upper subscript z in the inductance, currents, and voltage matrices matrix indicates that equations consist of both 9PH-4PO and 3PH-12PO mode terms (i.e. $z = 9,3$). The mutual inductance of the stator-rotor matrix $[L_{sr}]_{m*m}^{z}$ and torque developed by the machine is depending on the angular displacement between the stator and rotor, that is, θ_r. The symbol p defines the derivative operator, $p = \mathrm{d}/\mathrm{d}t$.

$$\begin{aligned} \left[T_s^{z}\right] = S_1\sqrt{\frac{2}{9}} \begin{array}{c} d \\ q \\ x1 \\ y1 \\ x2 \\ \ldots. \\ 0 \end{array} \left| \begin{bmatrix} \cos\theta & \cos(\theta-\alpha^9) & \cos(\theta-2\alpha^9) & \cos(\theta-3\alpha^9) & \ldots. & \cos(\theta-8\alpha^9) \\ \sin\theta & \sin(\theta-\alpha^9) & \sin(\theta-2\alpha^9) & \sin(\theta-3\alpha^9) & \ldots. & \sin(\theta-8\alpha^9) \\ \cos 2\theta & \cos 2(\theta-\alpha^9) & \cos 2(\theta-2\alpha^9) & \cos 2(\theta-3\alpha^9) & \ldots. & \cos 2(\theta-8\alpha^9) \\ \sin 2\theta & \sin 2(\theta-\alpha^9) & \sin 2(\theta-2\alpha^9) & \sin 2(\theta-3\alpha^9) & \ldots. & \sin 2(\theta-8\alpha^9) \\ \cos 3\theta & \cos 3(\theta-\alpha^9) & \cos 3(\theta-2\alpha^9) & \cos 3(\theta-3\alpha^9) & \ldots. & \cos 3(\theta-8\alpha^9) \\ \ldots. & \ldots. & \ldots. & \ldots. & \ldots. & \ldots. \\ \frac{1}{\sqrt{2}} & \frac{1}{\sqrt{2}} & \frac{1}{\sqrt{2}} & \ldots. & \ldots. & \frac{1}{\sqrt{2}} \end{bmatrix} \right. \\ + S_2\sqrt{\frac{2}{27}} \begin{array}{c} d \\ q \\ 0 \\ d1 \\ q1 \\ \ldots. \\ 0 \end{array} \left| \begin{bmatrix} \cos\theta & \cos(\theta-\alpha^3) & \cos(\theta-2\alpha^3) & \cos(\theta-3\alpha^3) & \ldots. & \cos(\theta-8\alpha^3) \\ \sin\theta & \sin(\theta-\alpha^3) & \sin(\theta-2\alpha^3) & \sin(\theta-3\alpha^3) & \ldots. & \sin(\theta-8\alpha^3) \\ \frac{1}{\sqrt{2}} & \frac{1}{\sqrt{2}} & \frac{1}{\sqrt{2}} & \ldots. & \ldots. & \frac{1}{\sqrt{2}} \\ \cos\theta & \cos(\theta-\alpha^3) & \cos(\theta-2\alpha^3) & \cos(\theta-3\alpha^3) & \ldots. & \cos(\theta-8\alpha^3) \\ \sin\theta & \sin(\theta-\alpha^3) & \sin(\theta-2\alpha^3) & \sin(\theta-3\alpha^3) & \ldots. & \sin(\theta-8\alpha^3) \\ \ldots. & \ldots. & \ldots. & \ldots. & \ldots. & \ldots. \\ \frac{1}{\sqrt{2}} & \frac{1}{\sqrt{2}} & \frac{1}{\sqrt{2}} & \ldots. & \ldots. & \frac{1}{\sqrt{2}} \end{bmatrix} \right. \end{aligned} \tag{4}$$

2.1 | Transformation matrix

For implementing accurate control as well as for eliminating the time-varying components in modelling equations of a machine,

the phase variable model equations have to be transformed into two-dimensional orthogonal sub-planes (*dq*). The transformation matrix for the 9-phase PPMIM drive is given in Equation (4). In this equation, θ is the phase shift between the *d*-axis with the *a*-phase axis of the stator. The transformation matrix has the following properties,

(i) *9PH-4PO mode*:
- ➢ The *dq* components in the first orthogonal plane (first two rows for Equation (4)) are responsible for torque production as well as airgap flux. In this plane, the dominant harmonics are of order $18k \pm 1$ ($k = 1,2,3,\ldots$).
- ➢ Other three orthogonal planes are responsible for the harmonic torques and are not responsible for airgap flux. The second, third, and fourth orthogonal planes consist of the harmonics $14k \pm 1$, $10k \pm 1$, and $6k \pm 1$, respectively ($k = 1,2, \ldots$).
- ➢ Only one zero sequence component exists.

(ii) *3PH-12PO mode*:
- ➢ Each effective phase consists of three identical windings, that is, the *R* phase is a combination of *a, d*, and *g* windings. So three in-phase *dq* components, that is, only one resultant orthogonal plane exists.
- ➢ The torque of the machine is directly proportional to the number of poles ($T \alpha P$). Based on this relation, the torque in this mode will be increased by three times as compared to the 9PH-4PO mode [7–13].
- ➢ The torque, as well as air gap flux, is produced with the three *dq* components, that is, with one resultant component.
- ➢ The dominant harmonics are of order $6k \pm 1$ ($k = 1, 2, 3,\ldots$).
- ➢ Three zero sequence components exist.

The equation for converting stator phase variable equations into *dq* domain and vice versa is as follows:

$$\left[f^{z}_{d,q,x1,x2\ldots0}\right] = [T_s]\left[f^{z}_{a,b,c,d\ldots i}\right] \tag{5}$$

$$\left[f^{z}_{a,b,c,d\ldots.i}\right] = [T_s]^{-1}\left[f^{z}_{d,q,x1,x2\ldots0}\right] \tag{6}$$

Here $[T_s]$ is Park's transformation matrix and $[T_s]^{-1} = [T_s]^{T}$ is the inverse transformation matrix. In Equations (5) and (6), the matrix $[f^{z}_{d,q,x1,x2\ldots0}]$ is the two-dimensional orthogonal plane representation and $[f_{a,b,c\ldots i}]$ is the actual phase variable matrix. For transforming the rotor phase variable equations into the *dq0* domain, the phase displacement between the rotor axis and to *dq0* axis is $\beta = \theta - \theta_r$ is to be considered in Equations (4), (5), and (6).

2.2 | Modelling equations in the arbitrary reference frame

The dynamic modelling of an electrical machine consists of voltage, flux linkage, electromagnetic torque, and mechanical torque equations. The stator and rotor voltage equations of the 9-phase PPMIM drive in the arbitrary reference frame are given in Equations (7) to (15) and (16) to (24), respectively, which are derived by using Equations (1) to (6).

$$S_1V^9_{ds} + S_2V^3_{ds} = R_s\left(S_1i^9_{ds} + S_2i^3_{ds}\right) + p\left(S_1\lambda^9_{ds} + S_2\lambda^3_{ds}\right) - \omega(S_1\lambda^9_{qs} + S_2\lambda^3_{qs}) \tag{7}$$

$$S_1V^9_{qs} + S_2V^3_{qs} = R_s\left(S_1i^9_{qs} + S_2i^3_{qs}\right) + p\left(S_1\lambda^9_{qs} + S_2\lambda^3_{qs}\right) + \omega\left(S_1\lambda^9_{ds} + S_2\lambda^3_{ds}\right) \tag{8}$$

$$S_1V^9_{x1s} + S_2V^3_{0s} = R_s\left(S_1i^9_{x1s} + S_2i^3_{0s}\right) + p\left(S_1\lambda^9_{x1s} + S_2\lambda^3_{0s}\right) \tag{9}$$

$$S_1V^9_{y1s} + S_2V^3_{d1s} = R_s\left(S_1i^9_{y1s} + S_2i^3_{d1s}\right) + p\left(S_1\lambda^9_{y1s} + S_2\lambda^3_{d1s}\right) - S_2\omega\lambda^3_{q1s} \tag{10}$$

$$S_1V^9_{x2s} + S_2V^3_{q1s} = R_s\left(S_1i^9_{x2s} + S_2i^3_{q1s}\right) + p\left(S_1\lambda^9_{x2s} + S_2\lambda^3_{q1s}\right) + S_2\omega\lambda^3_{d1s} \tag{11}$$

$$S_1V^9_{y2s} + S_2V^3_{0s} = R_s\left(S_1i^9_{y2s} + S_2i^3_{0s}\right) + p\left(S_1\lambda^9_{y2s} + S_2\lambda^3_{0s}\right) \tag{12}$$

$$S_1V^9_{x3s} + S_2V^3_{d2s} = R_s(S_1i^9_{x3s} + S_2i^3_{d2s}) + p(S_1\lambda^9_{x3s} + S_2\lambda^3_{d2s}) - S_2\omega\lambda^3_{q2s} \tag{13}$$

$$S_1V^9_{y3s} + S_2V^3_{q2s} = R_s\left(S_1i^9_{y3s} + S_2i^3_{q2s}\right) + p\left(S_1\lambda^9_{y3s} + S_2\lambda^3_{q2s}\right) + S_2\omega\lambda^3_{d2s} \tag{14}$$

$$S_1V^9_{0s} + S_2V^3_{0s} = R_s\left(S_1i^9_{0s} + S_2i^3_{0s}\right) + p\left(S_1\lambda^9_{0s} + S_2\lambda^3_{0s}\right) \tag{15}$$

$$S_1V^9_{dr} + S_2V^3_{dr} = 0 = R_r\left(S_1i^9_{dr} + S_2i^3_{dr}\right) + p\left(S_1\lambda^9_{dr} + S_2\lambda^3_{dr}\right) - (\omega - \omega_r)\left(S_1\lambda^9_{qr} + S_2\lambda^3_{qr}\right) \tag{16}$$

$$S_1V^9_{qr} + S_2V^3_{qr} = 0 = R_r\left(S_1i^9_{qr} + S_2i^3_{qr}\right) + p\left(S_1\lambda^9_{qr} + S_2\lambda^3_{qr}\right) + (\omega - \omega_r)\left(S_1\lambda^9_{dr} + S_2\lambda^3_{dr}\right) \tag{17}$$

$$S_1V^9_{x1r} + S_2V^3_{0r} = 0 = R_r\left(S_1i^9_{x1r} + S_2i^3_{0r}\right) + p\left(S_1\lambda^9_{x1r} + S_2\lambda^3_{0r}\right) \tag{18}$$

$$S_1V^9_{y1r} + S_2V^3_{d1r} = 0 = R_r\left(S_1i^9_{y1r} + S_2i^3_{d1r}\right) + p\left(S_1\lambda^9_{y1r} + S_2\lambda^3_{d1r}\right) - S_2(\omega - \omega_r)\lambda^3_{q1r} \tag{19}$$

$$S_1V^9_{x2r} + S_2V^3_{q1r} = 0 = R_r\left(S_1i^9_{x2r} + S_2i^3_{q1r}\right) + p\left(S_1\lambda^9_{x2r} + S_2\lambda^3_{q1r}\right) + S_2(\omega - \omega_r)\lambda^3_{d1r} \tag{20}$$

$$S_1V^9_{y2r}+S_2V^3_{0r}=0=R_r\left(S_1i^9_{y2r}+S_2i^3_{0r}\right)+p\left(S_1\lambda^9_{y2r}+S_2\lambda^3_{0r}\right) \tag{21}$$

$$S_1V^9_{x3r}+S_2V^3_{d2r}=0=R_r\left(S_1i^9_{x3r}+S_2i^3_{d2r}\right)+p\left(S_1\lambda^9_{x3r}+S_2\lambda^3_{d2r}\right)-S_2(\omega-\omega_r)\lambda^3_{q2r} \tag{22}$$

$$S_1V^9_{y3r}+S_2V^3_{q2r}=0=R_r\left(S_1i^9_{y3r}+S_2i^3_{q2r}\right)+p(S_1\lambda^9_{y3r}+S_2\lambda^3_{q2r})+S_2(\omega-\omega_r)\lambda^3_{d2r} \tag{23}$$

$$S_1V^9_{0r}+S_2V^3_{0r}=0=R_r\left(S_1i^9_{0r}+S_2i^3_{0r}\right)+p\left(S_1\lambda^9_{0r}+S_2\lambda^3_{0r}\right) \tag{24}$$

In Equations (7) to (24), ω and ω_r are the speed of *dq0* reference axis and rotor reference axis, respectively. The derivative operator is p. The flux linkage is the product of inductance and currents. The stator and rotor flux linkage equations of the 9-phase PPMIM drive are given in Equations (25) to (33) and (34) to (42), respectively.

$$S_1\lambda^9_{ds}+S_2\lambda^3_{ds}=S_1\left(L^9_{ls}+L^9_M\right)i^9_{ds}+S_2(L^3_{ls}+L^3_M)i^3_{ds}+S_1L^9_Mi^9_{dr}+S_2L^3_Mi^3_{dr} \tag{25}$$

$$S_1\lambda^9_{qs}+S_2\lambda^3_{qs}=S_1\left(L^9_{ls}+L^9_M\right)i^9_{qs}+S_2\left(L^3_{ls}+L^3_M\right)i^3_{qs}+S_1L^9_Mi^9_{qr}+S_2L^3_Mi^3_{qr} \tag{26}$$

$$S_1\lambda^9_{x1s}+S_2\lambda^3_{0s}=S_1\left(L^9_{ls}\right)i^9_{x1s}+S_2\left(L^3_{ls}\right)i^3_{0s} \tag{27}$$

$$S_1\lambda^9_{y1s}+S_2\lambda^3_{d1s}=S_1\left(L^9_{ls}\right)i^9_{y1s}+S_2\left(L^3_{ls}+L^3_M\right)i^3_{d1s}+S_2L^3_Mi^3_{d1r} \tag{28}$$

$$S_1\lambda^9_{x2s}+S_2\lambda^3_{q1s}=S_1\left(L^9_{ls}\right)i^9_{x2s}+S_2\left(L^3_{ls}+L^3_M\right)i^3_{q1s}+S_2L^3_Mi^3_{q1r} \tag{29}$$

$$S_1\lambda^9_{y2s}+S_2\lambda^3_{0s}=S_1\left(L^9_{ls}\right)i^9_{y2s}+S_2\left(L^3_{ls}\right)i^3_{0s} \tag{30}$$

$$S_1\lambda^9_{x3s}+S_2\lambda^3_{d2s}=S_1\left(L^9_{ls}\right)i^9_{x3s}+S_2\left(L^3_{ls}+L^3_M\right)i^3_{d2s}+S_2L^3_Mi^3_{d2r} \tag{31}$$

$$S_1\lambda^9_{y3s}+S_2\lambda^3_{q2s}=S_1\left(L^9_{ls}\right)i^9_{y3s}+S_2\left(L^3_{ls}+L^3_M\right)i^3_{q2s}+S_2L^3_Mi^3_{q2r} \tag{32}$$

$$S_1\lambda^9_{0s}+S_2\lambda^3_{0s}=S_1\left(L^9_{ls}\right)i^9_{0s}+S_2\left(L^3_{ls}\right)i^3_{0s} \tag{33}$$

$$S_1\lambda^9_{dr}+S_2\lambda^3_{dr}=S_1\left(L^9_{lr}+L^9_M\right)i^9_{dr}+S_2\left(L^3_{lr}+L^3_M\right)i^3_{dr}+S_1L^9_Mi^9_{ds}+S_2L^3_Mi^3_{ds} \tag{34}$$

$$S_1\lambda^9_{qr}+S_2\lambda^3_{qr}=S_1\left(L^9_{lr}+L^9_M\right)i^9_{qr}+S_2\left(L^3_{lr}+L^3_M\right)i^3_{qr}+S_1L^9_Mi^9_{qs}+S_2L^3_Mi^3_{qs} \tag{35}$$

$$S_1\lambda^9_{x1r}+S_2\lambda^3_{0r}=S_1\left(L^9_{lr}\right)i^9_{x1r}+S_2\left(L^3_{lr}\right)i^3_{0r} \tag{36}$$

$$S_1\lambda^9_{y1r}+S_2\lambda^3_{d1r}=S_1\left(L^9_{lr}\right)i^9_{y1r}+S_2\left(L^3_{lr}+L^3_M\right)i^3_{d1r}+S_2L^3_Mi^3_{d1s} \tag{37}$$

$$S_1\lambda^9_{x2r}+S_2\lambda^3_{q1r}=S_1\left(L^9_{ls}\right)i^9_{x2r}+S_2\left(L^3_{lr}+L^3_M\right)i^3_{q1r}+S_2L^3_Mi^3_{q1s} \tag{38}$$

$$S_1\lambda^9_{y2r}+S_2\lambda^3_{0r}=S_1\left(L^9_{lr}\right)i^9_{y2r}+S_2\left(L^3_{lr}\right)i^3_{0r} \tag{39}$$

$$S_1\lambda^9_{x3r}+S_2\lambda^3_{d2r}=S_1\left(L^9_{ls}\right)i^9_{x3r}+S_2\left(L^3_{lr}+L^3_M\right)i^3_{d2r}+S_2L^3_Mi^3_{d2s} \tag{40}$$

$$S_1\lambda^9_{y3r}+S_2\lambda^3_{q2r}=S_1\left(L^9_{lr}\right)i^9_{y3r}+S_2\left(L^3_{lr}+L^3_M\right)i^3_{q2r}+S_2L^3_Mi^3_{q2s} \tag{41}$$

$$S_1\lambda^9_{0r}+S_2\lambda^3_{0r}=S_1\left(L^9_{lr}\right)i^9_{0r}+S_2\left(L^3_{lr}\right)i^3_{0r} \tag{42}$$

In Equations (25) to (42), $L^{\tilde{z}}_{ls}$ and $L^{\tilde{z}}_M$ are the leakage and mutual inductances of the PPMIM drive, where $\tilde{z}=3,9$. The mutual inductance of the PPMIM machine in 9PH-4PO mode is $L^9_M=(9/2)L^9_{ms}$ and in 3PH-12PO mode is $L^3_M=(9/2)L^3_{ms}$. The value $L^{\tilde{z}}_{ms}$ is the magnetizing inductance of the PPMIM drive. The generated electromagnetic torque and mechanical torque equations of the PPMIM drive are given in Equations (43) and (44), respectively.

$$T_e=\frac{P}{2}\left(S_1L^9_M+S_2L^3_M\right)\times\left\{\begin{array}{l}\left(\begin{array}{l}\left[S_1i^9_{qs}+S_2\left(i^3_{qs}+i^3_{q1s}+i^3_{q2s}\right)\right]*\\ \left[S_1i^9_{dr}+S_2\left(i^3_{dr}+i^3_{d1r}+i^3_{d2r}\right)\right]\end{array}\right)\\ -\left(\begin{array}{l}\left[S_1i^9_{ds}+S_2\left(i^3_{ds}+i^3_{d1s}+i^3_{d2s}\right)\right]\\ *\left[S_1i^9_{qr}+S_2\left(i^3_{qr}+i^3_{q1r}+i^3_{q2r}\right)\right]\end{array}\right)\end{array}\right\} \tag{43}$$

$$T_e-T_L=J\left(\frac{2}{P}\right)\frac{\mathrm{d}\omega}{\mathrm{dt}}+B\left(\frac{2}{P}\right)\omega \tag{44}$$

where T_e is electromagnetic torque, T_L load torque, J is the inertia of moving parts (kg.m^2), B is the friction coefficient (lbm.ft^2), P is the number of poles, and ω is the angular speed of rotation. In Equation (43), *dq* currents of the PPMIM drive are

$$i^{\tilde{z}}_{ab}=S_1i^9_{ab}+S_2\left(i^3_{ab}+i^3_{a1b}+i^3_{a2b}\right) \tag{45}$$

where $a=d,q$ $b=s,r$

3 | IFOC OF PPMIM DRIVE

The vector control of the induction motor is derived from the DC separately excited machine torque equation, where the armature and field windings are designed in such a way that the currents will be orthogonal to each other with a decoupling nature. Similar to this concept, the IM is controlled with the *d*-axis flux component and *q*-axis torque component. The $d^s q^s$ axis of a stator is fixed with the stator axis, and the $d^r q^r$ axis of the rotor is fixed with the rotor axis and that is rotating at a speed of ω_r. The synchronous rotating $d^e q^e$ axis is rotating at a speed of ω_e, which is leading by an angle of θ_e and θ_r with respect to the stator and rotor reference axis. In the rotor field-oriented control, the field is aligned with a synchronously rotating $d^e q^e$ axis, with the knowledge of a field position. The relative speed, as well as the phase shift between the rotor reference axis ($d^r q^r$) to the rotor filed axis ($d^e q^e$), are,

$$\omega_{sl} = \omega_e - \omega_r \text{ and } \theta_{sl} = \theta_e - \theta_r \tag{46}$$

The rotor field axis is always in-phase with a synchronously rotating *d*-axis, that is, the orthogonal component is zero.

$$\lambda_{dr}^{e*} = \lambda_r^{\tilde{z}*} \text{ and } \lambda_{qr}^{e*} = 0 \tag{47}$$

$$\lambda_{dr}^{e*} p\lambda_{dr}^{e*} = \text{Constant, i.e., } = 0 \tag{48}$$

Equations (47) and (48) are standard equations for the indirect field-oriented vector control of the induction machine [2, 19]. These equations are derived based on the steady-state relations, and may not be valid for the transient conditions. For deriving the modelling equations for IFOC, machine modelling Equations (7) to (44) are analyzed in synchronous reference frame, that is, $\omega = \omega_e$. Substituting Equations (47) to (48) in the voltage and flux linkage equations of the rotor (16) to (24) and (34) to (42) gives the

$$S_1 i_{dr}^9 + S_2 i_{dr}^3 = 0, S_2 i_{d1r}^3 = 0 \text{ and } S_2 i_{d2r}^3 = 0 \tag{49}$$

$$S_1\lambda_{dr}^9 + S_2\lambda_{dr}^3 = S_1 L_M^9 i_{ds}^9 + S_2 L_M^3 i_{ds}^3 \tag{50}$$

$$S_2\lambda_{d1r}^3 = S_2 L_M^3 i_{d1s}^3 \tag{51}$$

$$S_2\lambda_{d2r}^3 = S_2 L_M^3 i_{d2s}^3 \tag{52}$$

$$R_r\left(S_1 i_{qr}^9 + S_2 i_{qr}^3\right) + \omega_{sl}\left(S_1\lambda_{dr}^9 + S_2\lambda_{dr}^3\right) = 0 \tag{53}$$

$$R_r S_2 i_{q1r}^3 + S_2\omega_{sl}\lambda_{d1r}^3 = 0 \tag{54}$$

$$R_r S_2 i_{q2r}^3 + S_2\omega_{sl}\lambda_{d2r}^3 = 0 \tag{55}$$

$$S_1\left(L_{lr}^9 + L_M^9\right) i_{qr}^9 + S_2\left(L_{lr}^3 + L_M^3\right) i_{qr}^3 = -\left(S_1 L_M^9 i_{qs}^9 + S_2 L_M^3 i_{qs}^3\right)\mathfrak{A} \tag{56}$$

$$S_2\left(L_{lr}^3 + L_M^3\right) i_{q1r}^3 = -S_2 L_M^3 i_{q1s}^3 \tag{57}$$

$$S_2\left(L_{lr}^3 + L_M^3\right) i_{q2r}^3 = -S_2 L_M^3 i_{q2s}^3 \tag{58}$$

In order to design a single control loop for regulating the flux of the 9-phase PPMIM drive, Equations (49) to (58) are rearranged as follows:

$$i_{dr}^{\tilde{z}} = 0 \tag{59}$$

$$\left(i_{ds}^{\tilde{z}}\right)^{e*} = \frac{S_1\lambda_{dr}^9 + S_2\lambda_{dr}^3}{S_1 L_M^9 + S_2 L_M^3} = \frac{\lambda_M^{\tilde{z}*}}{L_M^{\tilde{z}}}, \text{ where } G_1 = \frac{1}{L_M^{\tilde{z}}} \tag{60}$$

$$\omega_{sl} = -\frac{R_r i_{qr}^{\tilde{z}}}{\lambda_M^{\tilde{z}}} \tag{61}$$

$$i_{qr}^{\tilde{z}} = \frac{-L_M^{\tilde{z}} i_{qs}^{\tilde{z}}}{L_r^{\tilde{z}}} \tag{62}$$

The final slip equation is

$$\omega_{sl} = \frac{R_r}{L_r^{\tilde{z}}}\frac{L_M^{\tilde{z}}}{\lambda_M^{\tilde{z}}} i_{qs}^{\tilde{z}} \text{ where } G_4 = \frac{R_r}{L_r^{\tilde{z}}}\frac{L_M^{\tilde{z}}}{\lambda_M^{\tilde{z}}} = \frac{1}{\tau_r}\frac{1}{i_{ds}^{\tilde{z}}} \tag{63}$$

$$N_r^* = G_2\omega_r^* \text{ where } G_2 = P\pi/60 \tag{64}$$

The speed $NS_2 = 120f/P$, that is, 500 rpm for 3PH-12PO mode.

$$\left(i_{qs}^{\tilde{z}}\right)^{e*} = G_3 T_e \tag{65}$$

where

$$\mathrm{G}_3 = \frac{2}{P}\frac{L_r^{\tilde{z}}}{L_M^{\tilde{z}}}\frac{1}{\lambda_M^{\tilde{z}*}} \tag{66}$$

In the above Equations (59) to (66),
$L_b^{\tilde{z}} = S_1(L_{lb}^9 + L_M^9) + S_2(L_{lb}^3 + L_M^3), b = s, r, f^{\tilde{z}} = S_1(f^9) + S_2(f^3)$ where function *f* will be L_M, λ_M and other. In Equations (59) to (66) other cross-coupling terms (like $S_1 S_2 L_m^3 i_{ds}^9$, $S_1 S_2 L_m^9 i_{ds}^3$ and other) presented in Equations (49) to (58) are neglected.

The forward gains for *d*-axis component and *q*-axis components,

$$FG_d = -\omega_r\left[1 - \frac{\left(L_M^{\tilde{z}}\right)^2}{L_s^{\tilde{z}} L_r^{\tilde{z}}}\right] L_s^{\tilde{z}}\left(i_{qs}^{\tilde{z}}\right)^{e*} \tag{67}$$

$$FG_q = \omega_r L_s^{\tilde{z}}\left(i_{ds}^{\tilde{z}}\right)^{e*} \tag{68}$$

As discussed earlier in the 9-phase operation the windings are grouped into three sets of 3-phase windings. So in the implementation of IFOC for PPMIM drives, six currents are measured and other three currents are derived from the relation,

$$i_3 = -(i_1 + i_2) \text{ where } 3 = g, h, i; \quad 1 = a, b, c; \quad 2 = d, e, f \tag{69}$$

The complete block diagram of the IFOC of the PPMIM drive is shown in Figure 2. The vector control model is driven by the reference speed, and reference flux. From these inputs,

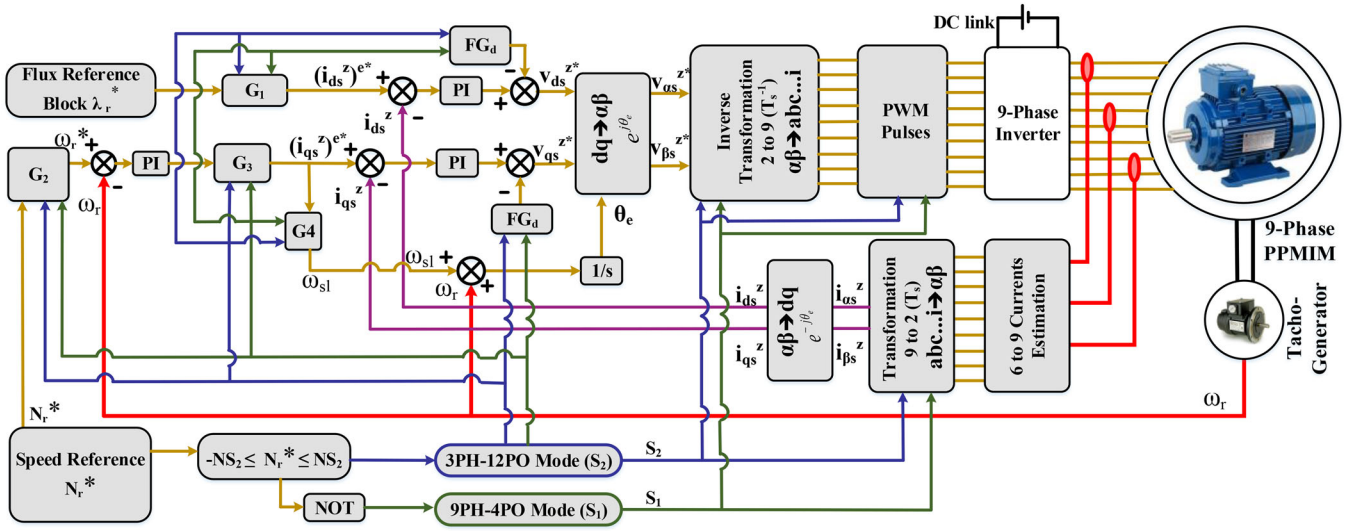

FIGURE 2 Block diagram of IFOC for 9-phase PPMIM drive. IFOC, indirect field-oriented control.

the controller generates the mode of operation, torque, and flux components. Here the torque and flux reference values are compared with actual values to generate tracking error. These errors are passed through respective PI loops to give stator *q*-axis and *d*-axis reference currents. These reference currents are compared with actual *dq* currents and the error is processed through the PI controller to attain the stator *q*-axis and *d*-axis voltage vectors. These voltage vectors are used to obtain reference stator phase voltages for driving the machine. For adding the compensation, the cross-coupling terms and transformations of variables have been used before generating actual stator phase voltages. These reference voltages are used to generate the PWM pulses for the 9-phase inverter-fed PPMIM drive.

4 | SIMULATION RESULTS AND DISCUSSION

A 5 hp 9-phase 4-pole PPMIM drive is implemented in MATLAB for validating the machine modelling equations presented in Section 2. The machine modelling is carried out in a stationary reference frame, that is, the speed of the *dq* axis, $\omega = 0$. The IFOC for the PPMIM machine has been implemented according to the equations given in Section 3 and the block diagram as shown in Figure 2. The 9-phase machine parameters used for the simulation are presented in the Appendix, which is the same for the experimental prototype. In the simulation study, a fixed step of 10 μs and the Runge Kutta, order-4 method is used for implementing the IFOC of the 9-phase PPMIM drive. A 9-phase two-level inverter presented in [28] is controlled using sinusoidal pulse width modulation (SPWM) at a switching frequency of 2 kHz. The PPMIM machine is controlled according to the speed reference input, which can be observed in Figure 2. The control logic for mode selection is as follows: if the reference speed N_r* satisfies the relation '$-NS_2 < N_r{}^* < NS_2$' (synchronous speed for 3PH-12PO mode is $NS_2 = 500$ rpm) then the machine will be operated in 3PH-12PO mode, that is, $S_1 = 0$ and $S_2 = 1$. Otherwise, the machine will operate in 9PH-4PO mode, that is, $S_1 = 1$ and $S_2 = 0$. During the transient condition, both pole phase modes will exist at the same time, that is, $S_1 = 1$ and $S_2 = 1$ for a predefined period of time.

In the MATLAB simulation, the speed reference is changed in the following order: (a) From $t = 0$ to 0.2 s, speed reference is kept at 0 rpm, (b) from $t = 0.2$ to 1 s, the speed reference is increased from 0 to 400 rpm, (c) from 1 to 2 s, the speed reference is increased to 1200 rpm, (d) from 2 to 2.7 s, the speed is reduced to 400 rpm and finally it is reduced to zero. According to the control logic, the drive will run in 3PH-12PO mode from 0 to 1 s and from 2 to 3 s. From 0.2 to 0.25 s the machine speed is increased linearly by applying maximum torque of 1.5 times of rated motor torque (dictated by the control algorithm). After 0.25 s, the machine speed increases linearly from 0 to 400 rpm and reaches the steady-state operation of 3PH-12PO mode that is shown in Figure 3. At 0.5 s, a step-change in load torque of 45 Nm is applied to the machine. This invokes the proposed IFOC and the machine torque accurately tracks the reference torque. The enlarged version of steady-state results for the 3PH-12PO mode is presented in Figure 4a, where the machine is operated at 400 rpm with a load torque of 45 Nm.

At 1 s, the speed reference is changed to 1200 rpm, that is, the mode of operation of PPMIM drive will change to 9PH-4PO mode. For maintaining the power constant in both pole phase modes, the torque is reduced to 15 Nm at 1 s. In MATLAB, it is not possible to emulate the magnetic behaviour of the machine, so an appropriate time for the reformation of poles, (i.e. 12 poles–4 poles) must be given. For this reason, the period of one electrical cycle is allowed for the torque, as well as speed commands to change linearly. The transient period for 3PH-12PO to 9PH-4PO modes changeover occurs during 1 to 1.04 s. During this period, both pole phase modes coexist. With the proposed IFOC, the torque/speed of the machine is controlled smoothly, that is, shown in Figures 3 and 4b. The steady-state

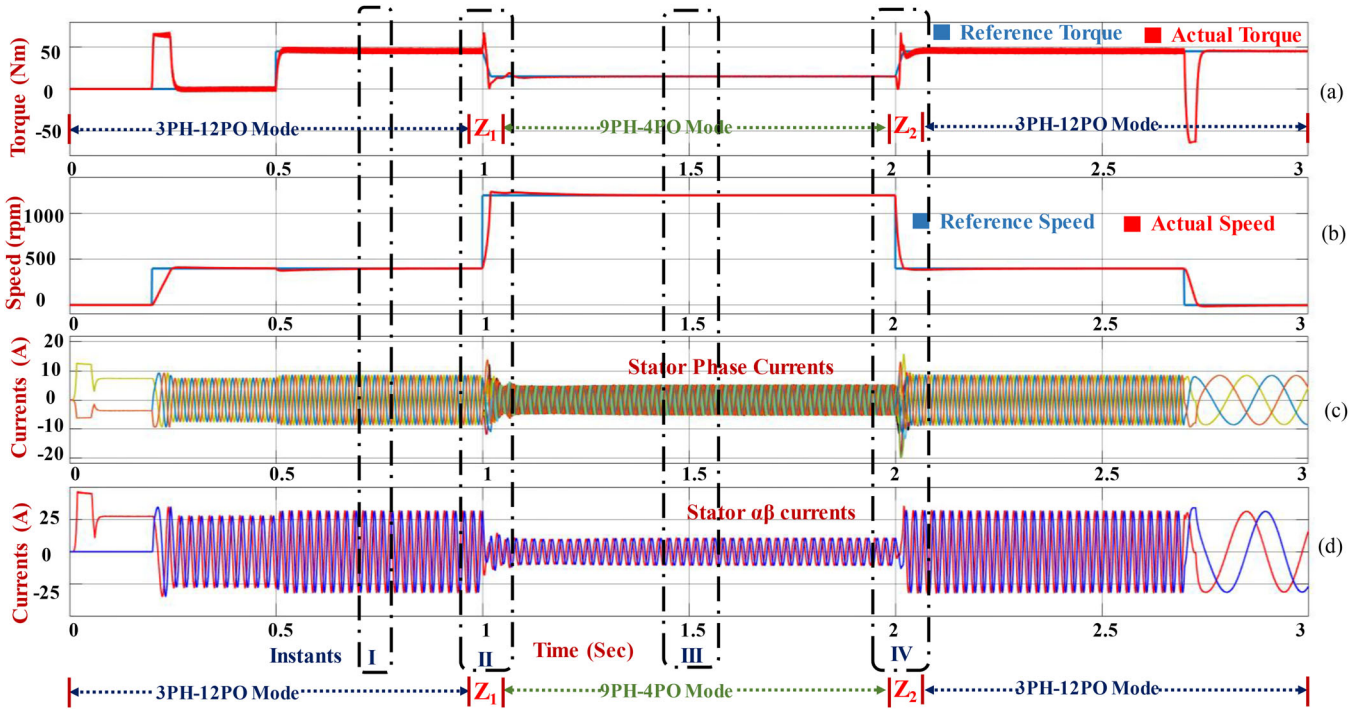

FIGURE 3 9-phase PPMIM drive simulated results with IFOC, (a) torque, (b) speed, (c) phase currents, (d) *dq* currents

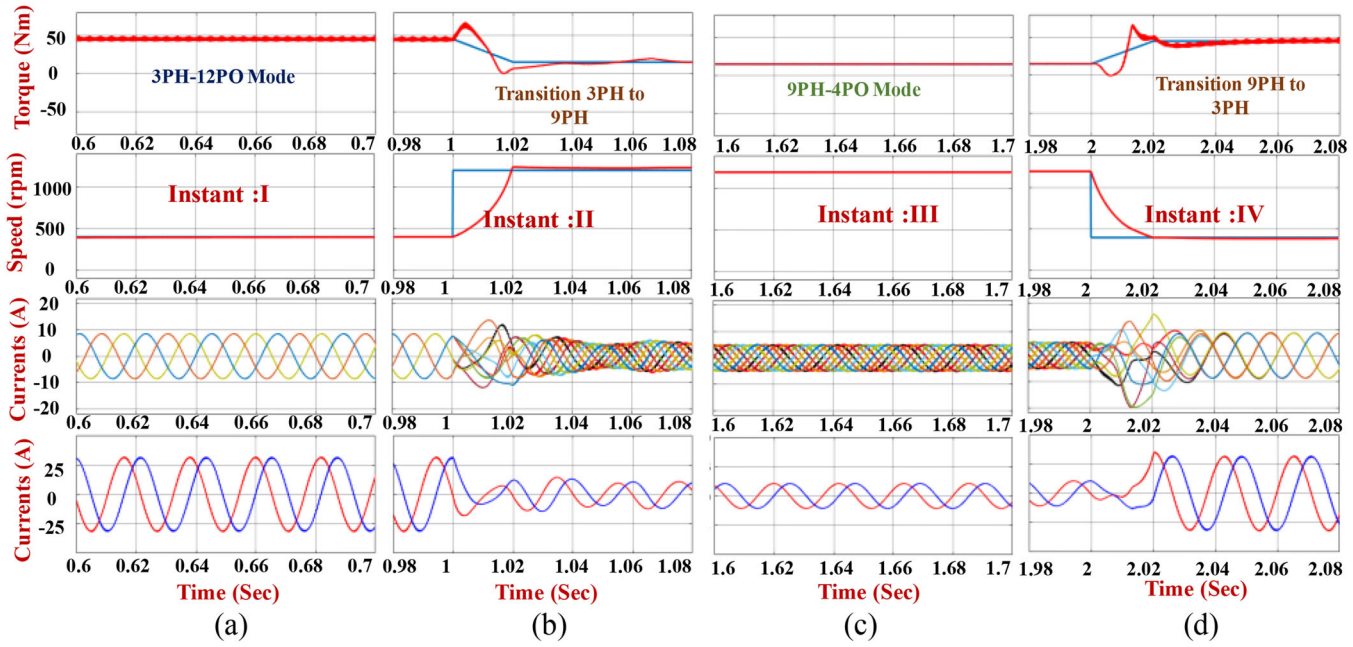

FIGURE 4 Enlarged view of 9-phase PPMIM drive simulated results at different instants with IFOC

results for the 9PH-4PO mode are shown in Figure 4c, where the drive is operated at 1200 rpm for a load torque of 15 Nm.

A step-change in speed reference is applied at 2 s, that is, speed reduced to 400 rpm and the drive operates in 3PH-12PO mode. The pole phase changeover period again exists from 2 to 2.04 s. The resulting waveforms are shown in Figures 3 and 4d. After the transient period, the steady-state of the 3PH-12PO mode exists from 2.04 to 2.7 s. The speed reference is changed to 0 rpm at 2.7 s but the load torque 45 Nm is applied, and the machine will decelerate linearly with 1.5 times of load torque (reverse side). During 2.7 to 3 s period, even though the reference speed is 0 rpm, the machine will run at very low speeds

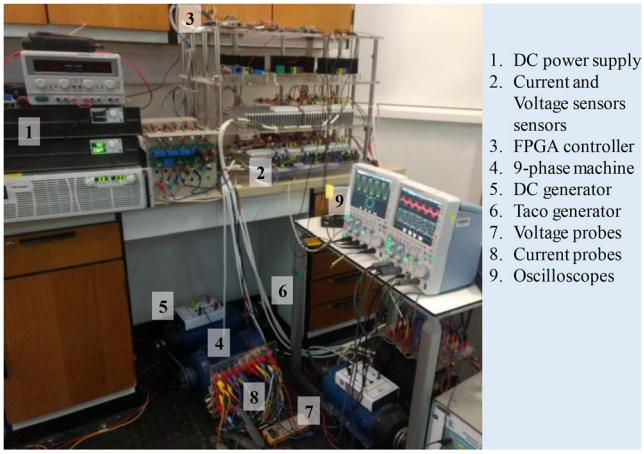

FIGURE 5 Laboratory prototype of 9-phase PPMIM drive

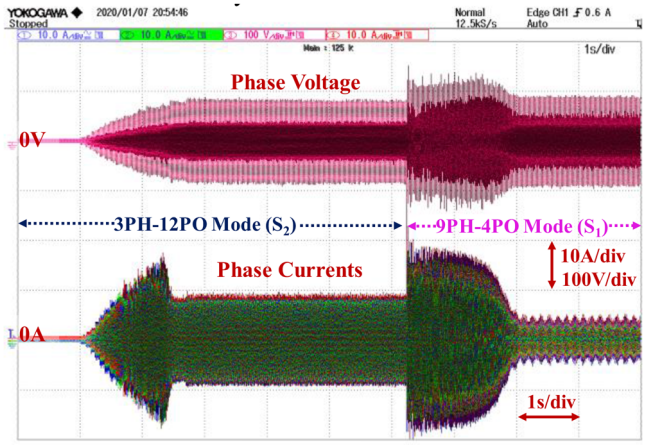

FIGURE 6 Experimental results of the PPMIM drive with open-loop *V/f* control

because of the load torque and inertia, that is, the slip frequency can be observed from the currents in Figure 3. From the results (shown in Figs. 3 and 4), it can be noticed that the PPMIM machine is accurately modelled and controlled during the steady-state as well as transient conditions of different pole phase combinations.

5 | EXPERIMENTAL RESULTS AND DISCUSSION

The experimental validation is performed on a 5 hp 4-pole 9phase 4pole IM laboratory setup. The machine design details and parameters are presented in the Appendix. A 1-kW DC machine is coupled with the 9-phase IM for loading. For sensing the speed, a tacho-generator is connected to the 9-phase IM shaft and its output is fed to the voltage sensor. For regulating the 9-phase IM speed/torque, a 9-phase 2-level inverter is designed in a laboratory with the help of 3-phase silicon carbide modules (CCS050M12CM2) and associated gate drives. In the experimental validation, six current sensors are used to achieve the nine currents of the machine. These currents are the feedback to the controller. The sum of three-phase currents related to the same 3-phase winding set is zero in 9PH-4PO mode, that is, the third current is realized with the equation $i_c = -(i_a + i_b)$. Whereas in 3PH-12PO mode, the winding currents in the same phase group are in-phase, so there is no need to realize third phase current. The proposed IFOC is implemented with the help of FPGA Vertex-5(XC5VLX50T), PMOD ADCs (AD7476A), DACs (AD5541A), and USM-3IV current/voltage sensors; the experimental prototype is presented in Figure 5. The base values considered for designing the control in FPGA are, $V_{dc} = 150$ V, current/phase (peak) = 10 A, $N_r = 3000$ rpm. The inverter is modulated with a 2-kHz switching frequency and SPWM.

The open-loop results of 9-phase PPMIM drive in both pole phase modes with *V/f* control are shown in Figure 6, where it can be observed that the transient current magnitude is twice that of steady-state current. In addition to this, current magnitudes are different in both pole phase modes due to the unequal fluxes and magnetizing inductance in the respective pole phase operation. This will degrade the machine's performance as well as lifespan. For improving the machine performance in both transient and steady state, an IFOC is implemented for the PPMIM drive (as shown in Figure 2). The experimental results of the PPMIM drive with IFOC are shown in Figures 7 and 8, where the phase voltage, current and speed (DAC outputs) for different modes are presented. The experimental current waveforms have lower order harmonics due to the uneven mechanical connectivity of the load DC machine.

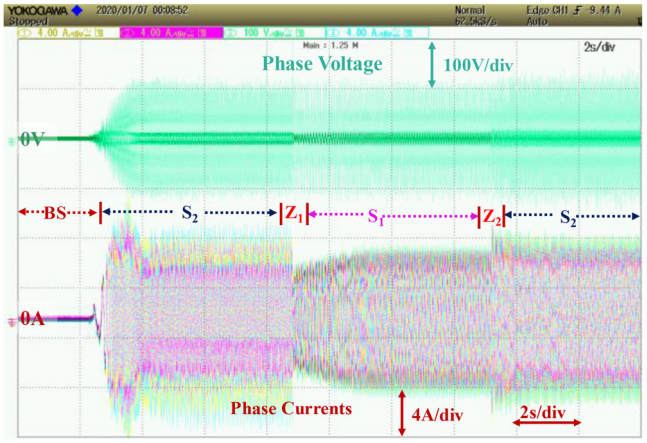

FIGURE 7 Experimental voltage and phase currents of PPMIM drive with IFOC

In Figure 7, a speed reference of 400 rpm is applied at 3 s, that is, the machine speed slowly increases. From 3 to 9 s, the speed reference is 400 rpm, so the machine operates in 3PH-12PO mode and the associated results are shown in Figures 7 and 9. From these figures, it is observed that the three-phase currents in the same 3-phase winding set are in-phase with each other. At 9 s, a step-change in speed from 400 to 1200 rpm is applied, due to this perturbation, the machine shifts to 9PH-4PO mode according to the control. The results during the

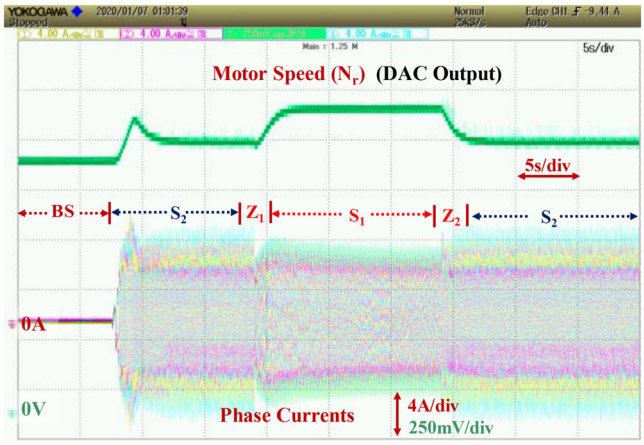

FIGURE 8 Experimental speed and phase currents of PPMIM drive with IFOC

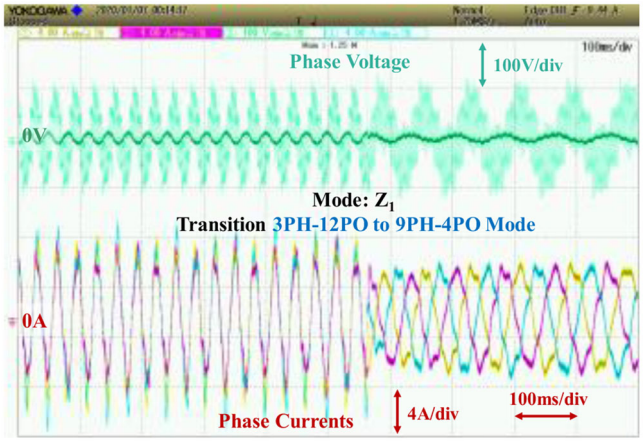

FIGURE 10 Experimental voltage and currents of PPMIM drive during transient mode Z_1 shown in Figure 6

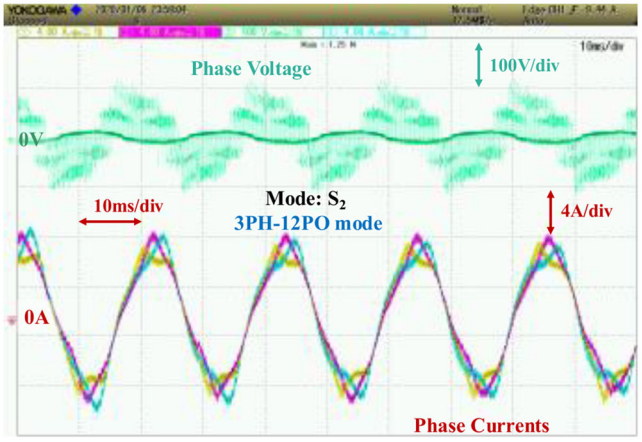

FIGURE 9 Steady-state voltage and currents of PPMIM drive in 3PH-12PO mode (S_2) with IFOC

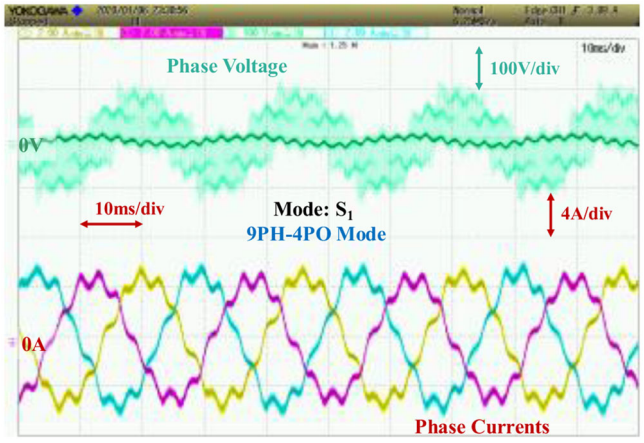

FIGURE 11 Steady-state voltage and currents of PPMIM drive in 9PH-4PO mode (S_1) with IFOC

transient period, that is, 3PH-12PO to 9PH-4PO mode pole changeover are shown in Figure 10. From this figure, it can be noticed that the current magnitudes are controlled within the rated per phase current limits. After the pole changeover, the machine tries to pick up the speed from 400 rpm in the 9PH-4PO operation, which can be observed from the frequency of the currents shown in Figure 10. The steady-state results of the 9PH-4PO mode are shown in Figure 11, where the machine is operated at 1200 rpm, that is, the frequency of the phase currents is 40 Hz and the phase shift between 3-phase currents in each 3-phase set is 120°. At 15 s, a step change in speed is applied, that is, from 1200 to 400 rpm, so the machine decelerates and operates in 3PH-12PO mode. The phase voltages and currents during the transient period (Z_2) of the PPMIM drive are shown in Figure 12.

The experimental speed plots (reference N_r^* and actual N_r) and reference stator voltages (V_α^*, V_β^* in stationary reference frame) are shown in Figure 13. The experimental V_α^*–V_β^* plots for 3PH-12PO and 9PH-4PO mode are shown in Figure 14. In these figures, the magnitudes of V_α^*, V_β^* are varied with respect to the variation in magnetizing inductances and speed reference in different modes of operation. The experimental d-axis (i_d^{e*} and i_d^e) and q-axis (i_q^{e*} and i_q^e) currents of the 9-phase PPMIM drive with IFOC are shown in Figure 15. In the vector control, the torque component is derived from the q-axis component. From Figure 15, it is noticed that the q-axis component has more ripple in the 3PH-12PO mode as compared to the 9PH-4PO mode. This is due to the lower magnetizing inductance in the 3PH-12PO mode, which is inversely proportional to the square of poles [15]. The detailed comparison of the proposed IFOC scheme with the respective pros and cons of different control techniques in the literature for PPM multiphase induction motor drives is presented in Table 1. From this comparison it can be noticed that the proposed control structure gives a better performance for variable pole phase induction motor drives.

In [10–13], many multilevel inverter configurations have been reported for 9-phase PPMIM drives which can be adopted for improving the torque ripple. In Figure 15, the d-axis components represent the flux component. From the results given in Figures 7, 8, and 15, it can be observed that the flux

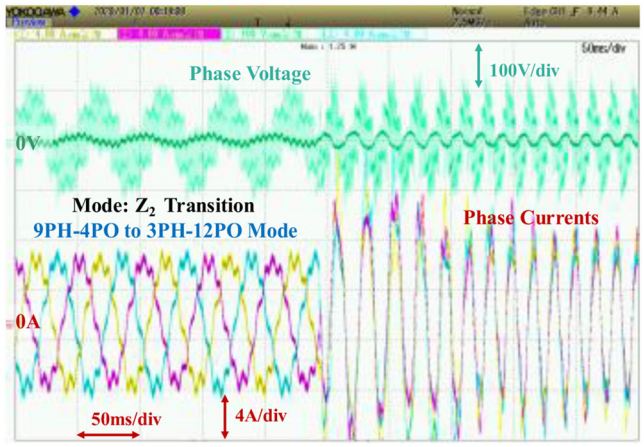

FIGURE 12 Experimental voltage and currents of PPMIM drive during transient mode Z_2 shown in Figure 6

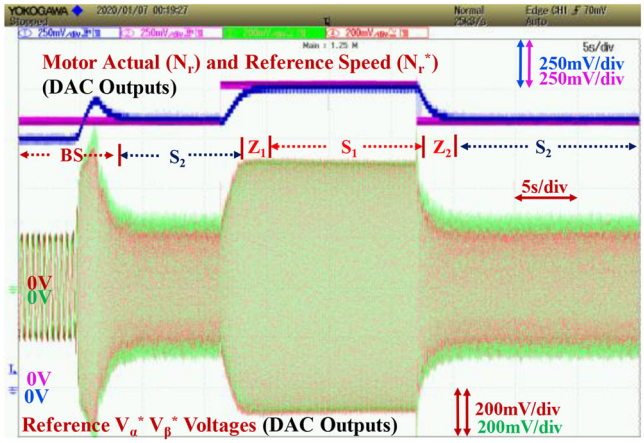

FIGURE 13 Speed (N_r and N_r^*) and reference voltages (V_α^*, V_β^*) of PPMIM drive (DAC outputs) with IFOC

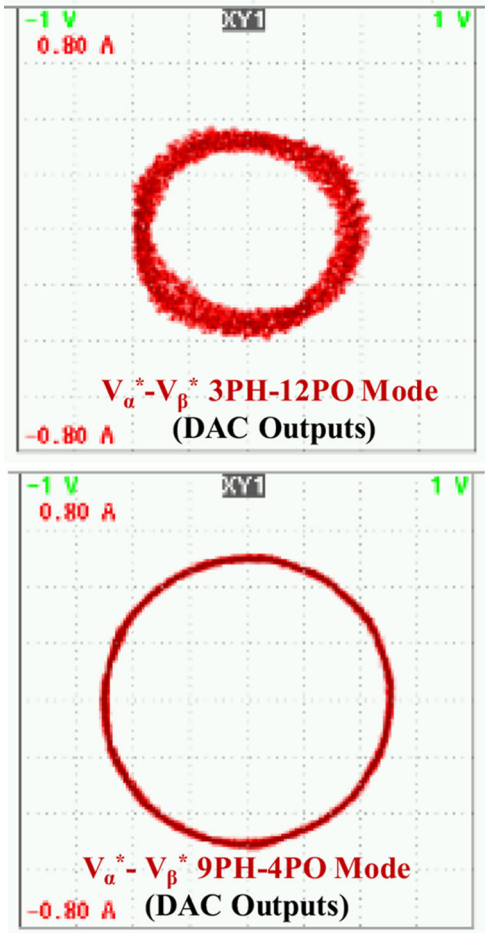

FIGURE 14 $V_\alpha^* - V_\beta^*$ plots of PPMIM drive

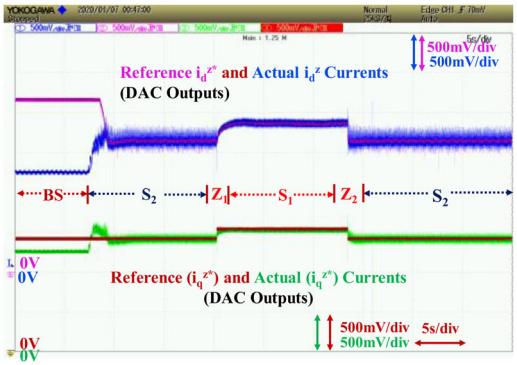

FIGURE 15 d-axis (i_d^{z*} and i_d^z) and q-axis (i_q^{z*} and i_q^z) currents of PPMIM drive (DAC outputs) with IFOC

component is maintained constant in the steady state of the respective pole phase mode of operation. However, in the transient state, the operating point changes continuously and reaches a steady state. From this, it can be concluded that Equations (47) and (48) are not valid for a short period of time due to a shift in operating point.

In the experimental setup, due to the limitation of power rating of external mechanical load (1-kW DC machine in this case), the experimental results shown correspond to the rated power for high-speed mode, that is, with no corresponding increase in the output torque during the low-speed mode. However, the power is constant in both pole phase modes ensuring that motor current during high-speed mode is proportionally lower for the same torque as compared to low-speed mode.

6 | CONCLUSION

Modelling, operation, and control of PPMIM drive during a transient as well as steady-state period is presented in this paper. The proposed mathematical model and control algorithm enhance the performance of the machine during a transient period by controlling the transient currents. This will help in improving the thermal management and lifespan of the machine. The modelling equations and IFOC are implemented with all the pole phase modes and can be easily extended for other PPMIM drives. The machine modelling equations of the 9-phase PPMIM drive are presented in an arbitrary reference

TABLE 1 Comparative study of the proposed IFOC for 9-phase PPM drives with other control schemes presented in the literature

Literature	Control scheme	Pros and cons	Results
[2]	**Indirect field-oriented control for multiphase machines**	**Pros** • Modelling for the m-phase machine is presented. • Generalized IFOC control for any multiphase machine similar to the 3-phase machine is presented. **Cons** • Modelling is not applicable for variable pole phase machines. • Control is not suitable for variable pole phase machines. • The flux linkages and inductance matrices will not be the same in all pole-phase operations. • The vector control techniques and transformation matrices should be the combination of all possible pole-phase combinations. • The decoupling components (like torque and flux components (i_d and i_q)) are different in magnitude.	Not applicable for pole phase modulated IM drives. This scheme is only applicable to individual multiphase machines
[8]	**Double vector control-based pole-changing control**	**Pros** • Pole changing has been done with double vector IFOC for 9-phase machines. • Speed and torque control are presented. **Cons** • Implemented individual control loops and modelling equations for **9phase 4pole** mode (9PH-4PO) and **3phase 12pole** (3PH-12PO) modes • Transformation matrices are not symmetrical (i.e. 4 to 9 is implemented) • The control, as well as the behaviour of the machine during the pole changeover, is poor. • Huge currents flowing in the transient condition. • Higher number of PI loops used. • Robustness of the control structure is less.	Presented in Figure 18 of the literature [8]
[25]	**Dual motor rotor-flux-oriented control**		Presented in Figure 8 of the literature [25]
[27]	**Hysteresis based IFOC of PPM based 9-phase IM drives**	**Pros** • Generalized dynamic mathematical model in phase variable as well as arbitrary reference frame by considering all possible pole and phase operations. • Symmetrical transformation matrices for converting 9 to 2 phase and 2 to 9 phase in both pole-phase modes. • Transient control of torque/speed during individual pole-phase modes as well as pole changeover conditions. **Cons** • Un-regulated switching frequency. • Current-based control. • Transient's behaviour and slower response. • Not applicable to do the different PWMs.	Presented in Figures 9–11 of the literature [27]
Proposed	**Voltage-based IFOC of PPM-based 9-phase IM drives**	**Pros** • Generalized single mathematical model in accordance with variable pole phase machines, like 9PH-4PO and 3PH-12PO modes has been presented. • A simple voltage-based IFOC for a 9-phase PPMIM drive is implemented for controlling the torque/speed. • Robust control structure with less sensitivity on PI tuning as compared to [8, 24, 27]. • Transient current magnitudes during pole changeover are minimized over [8, 24, 27]. • Fixed switching frequency any PWM can be applied. • The transient operation of the PPMIM drive during pole changeovers is accurately controlled.	Presented in Figures 7–13 in the revised paper

frame. The control logic for shifting the pole phase operation is derived based on the speed reference, which plays a crucial role in the proposed vector control. In 9-phase PPMIM drives, the torque components, as well as flux components, are derived with 1 *dq* component in 9PH-4PO mode and 3 *dq* components in 3PH-12PO mode. In this paper, the control is implemented with a single PI control loop for regulating the resultant torque and flux of the machine in all possible pole phase modes. The experimental and simulation results of the PPMIM drive show the effectiveness of the proposed control in steady state as well as pole changeover periods of different pole phase modes.

CONFLICT OF INTEREST

There is no conflict of interest.

FUNDING INFORMATION

This publication was made possible by QU High Impact Grant # [QUHI-CENG-19/20-2] from Qatar University. The statements made herein are solely the responsibility of the authors. Furthermore, this is to acknowledge that the publication charges of this article was funded by the Qatar National Library, Doha, Qatar.

DATA AVAILABILITY STATEMENT

Data sharing is not applicable to this article as no new data were created or analyzed in this study.

ORCID

Atif Iqbal https://orcid.org/0000-0002-6932-4367
B. Prathap Reddy https://orcid.org/0000-0002-6873-9624

REFERENCES

1. Duran, M.J., et al.: Multiphase energy conversion systems connected to microgrids with unequal power-sharing capability. IEEE Trans. Energy Convers. 32(4), 1386–1395 (2017)
2. Levi, E., et al.: Multiphase induction motor drives - a technology status review. IET Elec. Power Appl. 1(4), 489–516 (2007)
3. Subotic, I., et al.: Active and reactive power sharing between three-phase winding sets of a multiphase induction machine. IEEE Trans. Energy Convers. 34(3), 1401–1410 (2019)
4. Reddy, B.P., Keerthipati, S.: Multilayer fractional slot pole-phase modulated induction motor drives for traction applications. IEEE Trans. Ind. Electron. 67(11), 9112–9119 (2020)
5. Bodo, N., et al.: Efficiency evaluation of fully integrated on-board EV battery chargers with nine-phase machines. IEEE Trans. Energy Convers. 32(1), 257–266 (2017)
6. Liu, Z., Wu, J., Hao, L.: Coordinated and fault-tolerant control of tandem 15-phase induction motors in the ship propulsion system. IET Elec. Power Appl. 12(1), 91–97 (2018)
7. Umesh, B.S., Sivakumar, K.: 15 phase induction motor drive with 1:3:5 speed ratios using pole phase modulation. In: 2014 International Power Electronics Conference (IPEC-Hiroshima 2014 - ECCE ASIA), Hiroshima, pp. 1400–1404 (2014)
8. Ge, B., et al.: Winding design, modeling, and control for pole-phase modulation induction motors. IEEE Trans. Magn. 49(2), 898–911 (2013)
9. Prathap Reddy, B., et al.: A five speed 45-phase induction motor drive with pole phase modulation for electric vehicles. In: IEEE International Conference on Industrial Technology (ICIT), March 22–25, Toronto, pp. 258–263 (2017)
10. Reddy, B.P., Keerthipati, S.: A multilevel inverter configuration for an open-end-winding pole-phase-modulated-multiphase induction motor drive using dual inverter principle. IEEE Trans. Ind. Electron. 65(4), 3035–3044 (2018)
11. Prathap Reddy, B., et al.: A hybrid multilevel inverter scheme for nine-phase PPMIM drive by using three-phase five-leg inverters. IEEE Trans. Ind. Electron. 68(3), 1895–1904 (2021)
12. Bhimireddy, P.R., Keerthipati, S., Iqbal, A.: Phase reconfiguring technique for enhancing the modulation index of multilevel inverter fed nine-phase IM drive. IEEE Trans. Ind. Electron. 68(4), 2898–2906 (2021)
13. Reddy, B.P., Keerthipati, S.: Linear modulation range and torque ripple profile improvement of PPMIM drives. IEEE Trans. Power Electron. 34(12), 12120–12127 (2019)
14. Williamson, S., Smith, A.C.: Pulsating torque and losses in multiphase induction machines. IEEE Trans. Ind. Appl. 39(4), 986–993 (2003)
15. Munoz, R., Lipo, T.A.: Dual stator winding induction machine drive. IEEE Trans. Ind. Appl. 36(5), 1369–1379 (2000)
16. Peresada, S., Tilli, A., Tonielli, A.: Theoretical and experimental comparison of indirect field-oriented controllers for induction motors. IEEE Trans. Power Electron. 18(1), 151–163 (2003)
17. Barrero, F., Duran, M.J.: Recent advances in the design, modeling, and control of multiphase machines—Part I. IEEE Trans. Ind. Electron. 63(1), 449–458 (2016)
18. Levi, E., et al.: Modeling, control, and experimental investigation of a five-phase series-connected two-motor drive with single inverter supply. IEEE Trans. Ind. Electron. 54(3), 1504–1516 (2007)
19. Singh, G.K., Nam, K., Lim, S.K.: A simple indirect field-oriented control scheme for multiphase induction machine. IEEE Trans. Ind. Electron. 52(4), 1177–1184 (2005)
20. Prieto, I.G., et al.: Field-oriented control of multiphase drives with passive fault tolerance. IEEE Trans. Ind. Electron. 67(9), 7228–7238 (2020)
21. Mohapatra, K.K., et al.: Independent field-oriented control of two split-phase induction motors from a single six-phase inverter. IEEE Trans. Ind. Electron. 52(5), 1372–1382 (2005)
22. Iqbal, A., et al.: Indirect rotor flux oriented control of a seven-phase induction motor drive. In: 2006 IEEE International Conference on Industrial Technology, Mumbai, pp. 440–445 (2006). https://doi.org/10.1109/ICIT.2006.372203
23. de Souza, T.S., Bastos, R.R., Cardoso Filho, B.J.: Synchronous-frame modeling and dq current control of an unbalanced nine-phase induction motor due to open phases. IEEE Trans. Ind. Appl. 56(2), 2097–2106 (2002)
24. Kelly, J.W., Strangas, E.G., Miller, J.M.: Control of a continuously operated pole-changing induction machine. In: Proc. IEEE IEMDC, vol. 1, pp. 211–217 (2003)
25. Kelly, J.W., Strangas, E.G.: Torque control during pole-changing transition of a 3:1 pole induction machine. In: International Conference on Electrical Machines and Systems (CEMS), Seoul, pp. 1723–1728 (2007)
26. Prathap Reddy, B., et al.: Dynamic modelling and control of pole-phase modulation based multiphase induction motor drives. IEEE J. Emerg. Select Topics Power Electron. https://doi.org/10.1109/JESTPE.2021.3062216
27. Reddy, B.P., et al.: A single DC source-based three-level inverter topology for a four-pole open-end winding nine-phase PPMIM drives. IEEE Trans. Ind. Electron. 68(4), 2750–2759 (2021)
28. Reddy, B.P., Keerthipati, S.: Torque ripple minimization of PPMIM drives with phase-shifted carrier PWM. In: IECON 2018 44th Annual Conference of the IEEE Industrial Electronics Society, Washington, DC, pp. 725–730 (2018). https://doi.org/10.1109/IECON.2018.8591757

How to cite this article: Iqbal, A., Reddy, B.P., Rahman, S., Meraj, M.: Modelling and indirect field-oriented control for pole phase modulation induction motor drives. IET Power Electron. 1–13 (2022). https://doi.org/10.1049/pel2.12381